A Distributed Optimization Model for Mitigating Three-phase Power Imbalance with Electric Vehicles and Grid Battery

Liping Huang [a]; Dashen Chen [a]; Chun Sing Lai [a,b]; Zhaoxiong Huang [a]; Ahmed F. Zobaa [b]; Loi Lei Lai [a]

[a] Department of Electrical Engineering, School of Automation, Guangdong University of Technology, Guangzhou, China, 510006

[b] Brunel Interdisciplinary Power Systems Research Centre, Department of Electronic and Electrical Engineering, Brunel University London, Kingston Lane, London, UK, UB8 3PH

Corresponding author: chunsing.lai@brunel.ac.uk (C. S. Lai)

Abstract

Three-phase power imbalances may occur in the distribution network due to high electric vehicle (EV) charging demand. The imbalances become severe with the increasing number of EVs in the future and may be addressed with coordinated charging strategies. In this paper, we propose a phase-balancing and peak-shaving scheme for a community in the three-phase power distribution system by managing the charging and discharging strategies for EVs and grid battery energy storage systems (BESS). The proposed scheme includes energy transactions and distributed optimization models. In the transaction model, vehicle-to-vehicle (V2V) energy trading is considered. In the optimization model, the distribution system operator (DSO) optimizes the energy management strategy of the grid BESS while the EV owners optimize their charging strategies. Financial incentives are introduced to encourage the EV owners to assist the distribution system operator in reducing the phase imbalance. Simulation results show that the proposed scheme could mitigate the phase imbalance and reduce the difference between peak and valley load of the load curves in the three-phase distribution system. Both EV owners and the distribution system benefit financially. Moreover, the power quality and system reliability of the distribution network can also be improved.

Keywords: Three-phase power imbalance, phase balancing, battery energy storage system, electric vehicle, distributed optimization, energy transaction

1. Introduction

Three-phase four-wire networks are widely used in power distribution systems [1]. Residential customers are usually connected to the distribution system through single-phase lines. Due to the uneven allocation of single-phase load among three phases and the randomness of load behavior, phase imbalance is common in the distribution network. Phase balancing, i.e., keeping the load balanced in each phase is essential for the reliable and economic operation of the distribution system. This is because severe three-phase power imbalance will 1. increase line and transformer energy losses; 2. increase the risk of line tripping; 3. reduce power quality, energy efficiency, and the lifetime of induction motors. Ref. [2] provides a comprehensive review of the causes, consequences, and traditional solutions of phase imbalance in distribution networks.

In recent years, electric vehicles (EVs) are gaining popularity as the technology can potentially address internal combustion engine vehicle issues which contributes to fossil-fuel depletion, environmental problems, and lower running costs. As the number of plug-in EVs in the distribution system increases, the phase imbalance problem becomes increasingly serious due to the random nature of the travel and charging behavior of EV users [3]. A literature review on the impact of EV charging on the distribution network is presented in [4]. As the goal to achieve "carbon neutrality" as early as possible has become the consensus of most countries in the world, the number of EVs [5] connected to power grids will increase significantly in the future and the phase imbalance problem

may be aggravated and thus deserves more careful study. Coordinated charging strategies for EVs are needed. This not only helps to avoid phase imbalance caused by the EV users themselves but also helps to mitigate phase imbalance caused by other infeasible loads.

Many research projects have been done to solve the phase balancing problem. Traditionally, phase rebalancing techniques, such as phase swapping [6] and feeder reconfiguration [7] are widely used. However, these methods consider manual rephasing operation, which may be ineffective or can incur additional costs on human resources, maintenance expenses, and planned power outages. Recently, demand-side energy management strategies to mitigate phase imbalances have been investigated. The key idea is to use the power consumption flexibility of demand-side resources to balance the load. In [8], an active load control strategy is proposed to transfer load from the heavily loaded phase to the lightly loaded phase. As mentioned above, due to the presence of many plug-in EVs in the distribution system, strategies for coordinating EV charging are needed to avoid and mitigate the three-phase imbalance problem. Several studies have focused on this topic. In [9], the authors proposed an ordered charging strategy for electric vehicles in which the charging time, the size of charging power, and the amount of charging energy of each electric vehicle are uniformly scheduled to reduce the three-phase power imbalance. In [10], a real-time multilevel energy management strategy for EV charging is proposed. In this paper, both active and reactive charging power of EV chargers is optimized to balance power consumption in the three phases. In [11], the authors proposed a robust allocation approach of battery energy storage systems to improve the hosting capacity of unbalanced distribution networks including renewable energy generators. The

approaches mentioned above are all based on solving a centralized optimization problem. Although the centralized method is straightforward, two problems are associated with it. First, the customers are usually very careful while allowing the distribution system operator (DSO) to directly control their appliance because of privacy protection. Second, centralized optimization models suffer from "dimensional difficulties". As the number of customers increases, the efficiency of the solution decreases. To overcome these problems, distributed optimization models have been developed. In [12], a phase distributed balancing scheme based on the game-theoretic is proposed. The optimal control of energy storage systems has also been investigated to mitigate the power imbalance among phases in distribution networks. In [13], a stochastic optimization model for scheduling the charging and discharging power of the battery energy storage systems (BESS) is proposed to mitigate the phase imbalance in substations. Both centralized and distributed models are discussed in this paper. A distributed energy management strategy for community microgrids including energy storage systems is proposed in [14], where the maximum phase imbalance at the point of common coupling is constrained. The above literature shows that an ordered energy management strategy for EVs and BESS facilitates load balancing in the distribution system. However, there are still some shortcomings in the existing research work. In most of the distributed models presented in the above papers, the load balance constraint of the load bus and the power flow constraint of the distribution feeder are usually ignored, such as [10] and [12]. The optimal solutions obtained from these models may affect the reliable operation of the distribution system. In addition, none of these papers consider the cooperation of EVs and BESS to achieve

phase balancing. Although EVs and BESS have similar operation constraints, there are some differences in their models. Moreover, the randomness of EV charging also has negative impacts on the peak-valley difference of the load curve [15], [16], and [17]. The reduction of the peak-to-valley differences of active power consumption on each phase should be considered while dealing with the phase imbalance problem.

In summary, based on the above research gap analysis, this paper proposes a coordinated charging and discharging strategy for EVs and grid BESS to reduce the phase imbalance and peak-to-valley differences in the three-phase distribution system. This work is an extension of our previous work [18], in which an energy transaction model for mitigating three-phase power imbalance by scheduling EV charging is presented. Compared with existing studies and our previous work, the main contributions of this paper are summarized as follows:

1) We propose a phase-balancing and peak-shaving scheme for a three-phase power distribution system by managing the charging and discharging strategies for EVs and BESS. In the proposed scheme, an energy transaction model and a distributed optimization model are included.
2) In the transaction model, a vehicle-to-vehicle (V2V) energy trading mechanism is proposed. In the optimization model, both the centralized optimization method and the distributed optimization approach are proposed. The power flow constraints of the distribution feeders and the power balance constraint of the load bus are considered in the problem.
3) Financial incentives are introduced and allocated according to the contribution

of EVs and BESS to mitigate the three-phase imbalance and peak-to-valley differences. The benefits of our proposed scheme for EV owners, BESS, and the DSO are illustrated by extensive simulations.

4) Considering that some EV users may be reluctant to participate in coordinating charging strategies for commuting convenience, a scenario-based two-stage stochastic optimization model is proposed to cope with the load uncertainty caused by these EVs.

The rest of the paper is organized as follows. Section 2 introduces the system modeling and the proposed energy transaction model and optimization model. Consequently, a distributed optimization model is developed in Section 3. Section 4 introduces the scenario-based two-stage stochastic optimization model. Section 5 presents numerical results and discussions. Section 6 concludes the paper with future work given.

2. System Modeling and The Proposed Energy Transaction Model and Optimization Model

Fig. 1 shows a community in which single-phase uncontrollable loads, EV chargers, and grid BESS are connected to a load bus, while this bus is connected to the substation through the distribution feeder of a three-phase distribution system. Due to the random nature of load consumption and EV charging behavior, the power flow in the three-phase distribution feeders can be highly unbalanced. Since many EVs especially those used for commuting will spend most of their time parked at home or the workplace, their charging times can be quite flexible. Therefore, the DSO can take advantage of the timing flexibility of EV charging and provide certain incentives to encourage rescheduling of

EV charging. This not only helps to avoid phase imbalance caused by EVs themselves but also helps to mitigate phase imbalance caused by other uncontrollable loads.

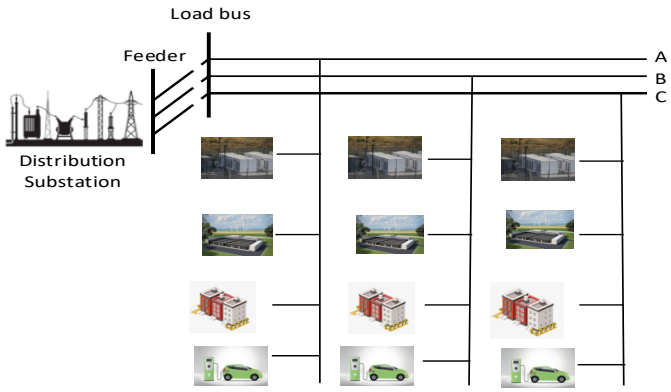

Fig. 1. A community connected to a three-phase distribution system

In this section, we describe the proposed energy transaction model and the optimization model. These models help mitigate the phase imbalance and peak-to-valley differences in the three-phase load profile, by coordinating the charging and discharging of EVs and grid BESS.

2.1 Energy Transaction Model

To enhance the three-phase power balancing in the system, there is a requirement for additional development for new market designs to increase EVs' participation [19]. It is conceivable that if the price of EV charging from the grid is higher than the price of discharging to it, it is expected that electric vehicle owners will use these price signals to trade energy to make a profit or reduce charging costs. However, due to the decentralized nature of EVs, EVs that reach trading contracts need to trade energy through distribution networks. To reduce the three-phase imbalance, an agreement could be formed between the DSO and EVs: the DSO would waive the distribution fee for the EVs, while the charging and discharging phases for the EVs would be selected by the DSO. Based on the above analysis, Fig. 2 presents a V2V energy trading model based on a double auction

mechanism. Sellers and buyers are ranked based on the offer information, with sellers ranking high if they have a low bid and buyers ranking high if they have a high bid. The vertical dashed line indicates the auction breakpoint. The EV user to the left of the auction breakpoint will conclude the transaction contract. The DSO will arrange their final charging and discharging strategy. For example, if the load on phase A is heavy, the EV is scheduled to discharge on phase A. If the load on phase B is light, the EV is scheduled to charge on phase B. The EVs to the right of the auction breakpoint did not get a trade contract and some EVs do not want to participate in V2V energy trading because frequent discharges can affect the life of the battery. These EVs can participate in the optimization model to reduce charging costs which will be discussed in the next section.

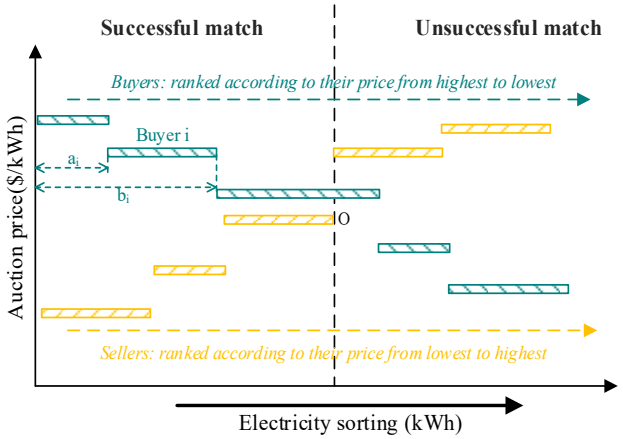

Fig. 2. Aggregation of bidding curve and determination of the bidding price.

2.2 The Centralized Optimization Model

In this section, by coordinating the charging and discharging of EVs and grid BESS, we present the mathematical formulation of the centralized optimization problem to mitigate the phase imbalance and peak-to-valley differences in the three-phase load profile. Before detailing the objectives and constraints of the optimization problem, we first describe the mathematical modeling of the system. Fig. 3 shows the power flow

distribution of the above distribution system, and the details in phase B are shown as an example. Note that for brevity, in the following discussion we use phases 1, 2, and 3 to denote phases A, B, and C, respectively. Fig. 3 shows that the power flow in the distribution feeders at time slot t is denoted as $P_{p,t}^{\text{Grid}}$ $\left(p=\{1,2,3\}\right)$. The key idea of this work is to minimize the differences between the power flow in each phase and each time slot. Note that we assume the value of $P_{p,t}^{\text{Grid}}$ is always positive, i.e., the load consumption of the distribution system is assumed to be greater than the production. In each phase, the amount of active power consumption of the uncontrollable load at time slot t is denoted as $P_{p,t}^{\text{Load}}$. Assume that there are NEV_p EVs, NBS_p grid BESS units in phase p. The charging power of the i-th EV of phase p at time slot t is denoted as $P_{p,i,t}^{\text{EVch}}$. The charging and discharging power of the j-th BESS unit of phase p at time slot t are denoted as $P_{p,j,t}^{\text{BSch}}$ and $P_{p,j,t}^{\text{BSdis}}$, respectively. With these definitions, we then introduce the mathematical formulation of the proposed optimization problem.

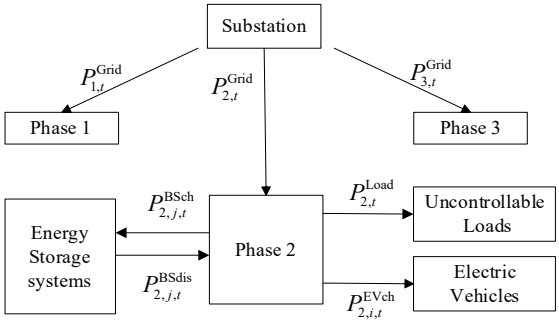

Fig. 3. Power flow distribution modeling of the three-phase distribution system.

The objective terms to minimize the phase imbalance and peak-to-valley differences of the three-phase load curves in the time horizon T are shown in Equation (1).

$$PIB=\sum_{t=1}^{T}\sum_{p=1}^{3}\left(P_{p,t}^{\text{Grid}}-\frac{1}{3}\sum_{p=1}^{3}P_{p,t}^{\text{Grid}}\right)^2,\quad TIB=\sum_{t=1}^{T}\sum_{p=1}^{3}\left(P_{p,t}^{\text{Grid}}-\frac{1}{T}\sum_{t=1}^{T}P_{p,t}^{\text{Grid}}\right)^2 \tag{1}$$

In (1), PIB reflects the variance of the power flow for the three phases, and TIB

reflects the variance of the power flow for different time slots in the time horizon. The smaller these two terms are, the more balanced the power flow is for the three phases and for all time slots. Thus, by minimizing them, we can reduce the phase imbalance and the peak-to-valley differences of the three-phase load curves. Together with the operating costs of EVs and BESS, the objective function of the proposed optimization model is shown in Equation (2).

$$\begin{aligned}\min\ & k^{\mathrm{Pib}}\sum_{t=1}^{T}\sum_{p=1}^{3}\left(P_{p,t}^{\mathrm{Grid}}-\frac{1}{3}\sum_{p=1}^{3}P_{p,t}^{\mathrm{Grid}}\right)^2+k^{\mathrm{Tib}}\sum_{t=1}^{T}\sum_{p=1}^{3}\left(P_{p,t}^{\mathrm{Grid}}-\frac{1}{T}\sum_{t=1}^{T}P_{p,t}^{\mathrm{Grid}}\right)^2\\ &+\sum_{t=1}^{T}\sum_{p=1}^{3}\sum_{i=1}^{NEV_p}p_t^{\mathrm{Price}}P_{p,i,t}^{\mathrm{EVch}}\Delta t\\ &+\sum_{t=1}^{T}\sum_{p=1}^{3}\sum_{j=1}^{NBS_p}p_t^{\mathrm{Price}}\left(P_{p,j,t}^{\mathrm{BSch}}-P_{p,j,t}^{\mathrm{BSdis}}\right)\Delta t\\ &+0.5\times\sum_{t=1}^{T}\sum_{p=1}^{3}\sum_{j=1}^{NBS_p}\frac{\left|\eta_{p,j}^{\mathrm{BSch}}P_{p,j,t}^{\mathrm{BSch}}-P_{p,j,t}^{\mathrm{BSdis}}/\eta_{p,j}^{\mathrm{BSdis}}\right|\times\Delta t}{\mathrm{L}_{cyc}^{80\%}}\times p_{bat}^{\mathrm{Price}}\end{aligned}\tag{2}$$

The second row of the objective function is the total charging cost of all EVs. The third and fourth rows are the cost of BESS, which is equal to the charging cost minus the discharge revenue, and then add the battery degradation cost [20]. For the constraints, the proposed model considers the power balance of the load bus and the flow limitations of each phase feeder, as well as the operating constraints of the EVs and BESS, as shown in Equations (3)-(17).

$$P_{p,t}^{\mathrm{Grid}}=P_{p,t}^{\mathrm{Load}}+\sum_{i=1}^{NEV_p}P_{p,i,t}^{\mathrm{EVch}}+\sum_{j=1}^{NBS_p}\left(P_{p,j,t}^{\mathrm{BSch}}-P_{p,j,t}^{\mathrm{BSdis}}\right),\ \forall p,\forall t\tag{3}$$

$$P_{p,t}^{\mathrm{Grid}}\le P_{p}^{\mathrm{GridMax}},\ \forall p,\forall t\tag{4}$$

$$0\le P_{p,i,t}^{\mathrm{EVch}}\le P_{p,i}^{\mathrm{EVmax}},\ \forall p,\forall i,\forall t\tag{5}$$

$$E_{p,i,t}^{\mathrm{EV}}=E_{p,i,t-1}^{\mathrm{EV}}+\Delta t\cdot\eta_{p,i}^{\mathrm{EVch}}\cdot P_{p,i,t}^{\mathrm{EVch}},\ \forall p,\forall i,\forall t\tag{6}$$

$$E_{p,i,0}^{\mathrm{EV}}=SoC_{p,i}^{\mathrm{EVIni}}E_{p,i}^{\mathrm{EVmax}},\ \forall p,\forall i\tag{7}$$

$$E_{p,i}^{\mathrm{EVmin}} \le E_{p,i,t}^{\mathrm{EV}} \le E_{p,i}^{\mathrm{EVmax}},\ \forall p, \forall i, \forall t \tag{8}$$

$$E_{p,i,\mathrm{T}}^{\mathrm{EV}} \ge SoC_{p,i}^{\mathrm{EVexp}} E_{p,i}^{\mathrm{EVmax}},\ \forall p, \forall i \tag{9}$$

$$0 \le P_{p,j,t}^{\mathrm{BSch}} \le y_{p,j,t}^{\mathrm{BSch}} \cdot P_{p,j}^{\mathrm{BSmax}},\ \forall p, \forall j, \forall t \tag{10}$$

$$0 \le P_{p,j,t}^{\mathrm{BSdis}} \le y_{p,j,t}^{\mathrm{BSdis}} \cdot P_{p,j}^{\mathrm{BSmax}},\ \forall p, \forall j, \forall t \tag{11}$$

$$y_{p,j,t}^{\mathrm{BSdis}} + y_{p,j,t}^{\mathrm{BSch}} \le 1,\ \forall p, \forall j, \forall t \tag{12}$$

$$y_{p,j,t}^{\mathrm{BSch}}, y_{p,j,t}^{\mathrm{BSdis}} \in \{0,1\},\ \forall p, \forall j, \forall t \tag{13}$$

$$E_{p,j,t}^{\mathrm{BS}} = E_{p,j,t-1}^{\mathrm{BS}} + \Delta t \cdot \eta_{p,j}^{\mathrm{BSch}} \cdot P_{p,j,t}^{\mathrm{BSch}} - \Delta t \cdot \frac{P_{p,j,t}^{\mathrm{BSdis}}}{\eta_{p,j}^{\mathrm{BSdis}}},\ \forall p, \forall j, \forall t \tag{14}$$

$$E_{p,j,\mathrm{T}}^{\mathrm{BS}} = E_{p,j,0}^{\mathrm{BS}},\ \forall p, \forall j \tag{15}$$

$$E_{p,j,0}^{\mathrm{BS}} = SoC_{p,j}^{\mathrm{BSIni}} E_{p,j}^{\mathrm{BSmax}},\ \forall p, \forall j \tag{16}$$

$$SoC_{p,j}^{\mathrm{BSmin}} E_{p,j}^{\mathrm{BSmax}} \le E_{p,j,t}^{\mathrm{BS}} \le SoC_{p,j}^{\mathrm{BSmax}} E_{p,j}^{\mathrm{BSmax}},\ \forall p, \forall j, \forall t \tag{17}$$

The power balance of each time slot in each phase is ensured by Equation (3). Constraint Equation (4) ensures power flow limitation of distribution feeders. For each EV, the minimum and maximum charging power are constrained by Equation (5), and the energy in the EV battery at the end of each time slot is calculated by Equations (6) and (7), and constrained by Equation (8). Constraint Equation (9) ensures that the final stored energy of the EV battery is greater than the expected value of the EV owner. For each BESS system, the constraints Equation (10) and Equation (11) limit the charging and discharging power of the BESS to the allowed range. Two integer variables are used to ensure that only one state, i.e., charging or discharging, is true during each time interval. Equation (14) calculates the energy in the BESS for each period considering the efficiency of charging and discharging, and Equation (15) ensures that the final stored energy in the BESS is equal to the initial energy. Constraint Equation (17) ensures that

the energy stored in the BESS is within the allowable operating range.

3. Distributed Optimization Algorithm for the Centralized Model

The centralized optimization model proposed in Section 2.2 is straightforward to implement. However, privacy issues may arise in practical implementation, as EV users may be unwilling to provide their information to the DSO. In addition, the solving efficiency of this model may decrease as the number of EVs increases. In this section, we provide a distributed algorithm to solve this centralized optimization model, where only a limited exchange of information is required. The distributed algorithm is based on the alternating direction method of multiplier (ADMM) [21]. In this paper, we decompose the centralized optimization model into optimization subproblems at the DSO and EV owner levels. The DSO optimizes the charging and discharging of the grid BESS and the power input from the grid, while the EV users optimize their charging power. The optimal solution can be found by iteratively exchanging and updating their solution results. As shown in Section 2, only the power balance constraint Equation (3) is a complex constraint that involves variables at both levels mentioned above. According to the scaled form of ADMM, by introducing a scaled dual variable $u_{p,t}$, we could decompose the centralized optimization problem into a set of optimization subproblems without coupling constraint Equation (3). The complete procedure of the proposed distributed optimization algorithm is shown in Algorithm 1.

Algorithm 1: Distributed Optimization Algorithm for the Proposed Model

1: **Initialization:** $P_{p,i}^{\mathrm{EVmax}}$, $\eta_{p,i}^{\mathrm{EVch}}$, $E_{p,i}^{\mathrm{EVmin}}$, $E_{p,i}^{\mathrm{EVmax}}$, $E_{p,i}^{\mathrm{EVexp}}$, $\eta_{p,j}^{\mathrm{BSch}}$, $\eta_{p,j}^{\mathrm{BSdis}}$, $P_{p,j}^{\mathrm{BSmax}}$, $E_{p,j}^{\mathrm{BSmax}}$, $E_{p,j,0}^{\mathrm{BS}}$, P_{p}^{GridMax}

2: Set the counter $k=0$, $P_{p,i,t}^{\mathrm{EVch},(k)}=0$ $P_{p,j,t}^{\mathrm{BSch},(k)}=0$, $P_{p,j,t}^{\mathrm{BSdis},(k)}=0$, $P_{p,t}^{\mathrm{Grid},(k)}=0$, $u_{p,t}^{(k)}=0$.

3: **repeat**

4: Solve **SubP1** Equation (18) for each EV and get the result $P_{p,i,t}^{\mathrm{EVch},(k+1)}$. Pass the solution result to **SubP2**.

5: Solve **SubP2** Equation (19) and get the result $P_{p,j,t}^{\mathrm{BSch},(k+1)}$, $P_{p,j,t}^{\mathrm{BSdis},(k+1)}$ and $P_{p,t}^{\mathrm{Grid},(k+1)}$. Pass the solution result to **SubP1**.

6: Update $u_{p,t}^{(k+1)}$, $r_{p,t}^{k+1}$ and $s_{p,t}^{k+1}$ by Equations (20) and (21).

7: $k=k+1$

8: **Until** $r_{p,t}^{k+1}\le\varepsilon^{pri}$ **and** $s_{p,t}^{k+1}\le\varepsilon^{dual}$

9: **Return** $P_{p,i,t}^{\mathrm{EVch}}$, $P_{p,j,t}^{\mathrm{BSch}}$, $P_{p,j,t}^{\mathrm{BSdis}}$, and $P_{p,t}^{\mathrm{Grid}}$.

In iteration $k+1$, the optimization subproblem for the i-th EV on phase p is as follows.

$$\begin{aligned}\textbf{SubP1:}\ &\min \sum_{t=1}^{T} p_t^{\mathrm{Price}} P_{p,i,t}^{\mathrm{EVch}} \Delta t \\ &+\frac{\rho}{2}\sum_{t=1}^{T}\sum_{p=1}^{3}\left\| P_{p,i,t}^{\mathrm{EVch}} + \sum_{n=1,n\neq i}^{NEV_p} P_{p,n,t}^{\mathrm{EVch},(k)} + \sum_{j=1}^{NBS_p}\left(P_{p,j,t}^{\mathrm{BSch},(k)} - P_{p,j,t}^{\mathrm{BSdis},(k)}\right) - P_{p,t}^{\mathrm{Grid},(k)} + P_{p,t}^{\mathrm{Load}} + u_{p,t}^{(k)} \right\|_2^2 \\ &\text{s.t. (5)-(9)}\end{aligned} \tag{18}$$

In iteration $k+1$, the optimization subproblem for the DSO is as follows:

$$\begin{aligned}\textbf{SubP2:}\ &\min k^{\mathrm{Pib}}\sum_{t=1}^{T}\sum_{p=1}^{3}\left(P_{p,t}^{\mathrm{Grid}} - \frac{1}{3}\sum_{p=1}^{3}P_{p,t}^{\mathrm{Grid}}\right)^2 + k^{\mathrm{Tib}}\sum_{t=1}^{T}\sum_{p=1}^{3}\left(P_{p,t}^{\mathrm{Grid}} - \frac{1}{T}\sum_{t=1}^{T}P_{p,t}^{\mathrm{Grid}}\right)^2 \\ &+\sum_{t=1}^{T}\sum_{p=1}^{3}\sum_{j=1}^{NBS_p} p_t^{\mathrm{Price}}\left(P_{p,j,t}^{\mathrm{BSch}} - P_{p,j,t}^{\mathrm{BSdis}}\right)\Delta t \\ &+0.5\times\sum_{t=1}^{T}\sum_{p=1}^{3}\sum_{j=1}^{NBS_p}\frac{\left|\eta_{p,j}^{\mathrm{BSch}}P_{p,j,t}^{\mathrm{BSch}} - P_{p,j,t}^{\mathrm{BSdis}}/\eta_{p,j}^{\mathrm{BSdis}}\right|\times\Delta t}{\mathrm{L}_{cyc}^{80\%}}\times p_{bat}^{\mathrm{Price}} \\ &+\frac{\rho}{2}\sum_{t=1}^{T}\sum_{p=1}^{3}\left\|\sum_{i=1}^{NEV_p}P_{p,i,t}^{\mathrm{EVch},(k+1)} + \sum_{j=1}^{NBS_p}\left(P_{p,j,t}^{\mathrm{BSch}} - P_{p,j,t}^{\mathrm{BSdis}}\right) - P_{p,t}^{\mathrm{Grid}} + P_{p,t}^{\mathrm{Load}} + u_{p,t}^{(k)}\right\|_2^2 \\ &\text{s.t. (4), (10)-(17)}\end{aligned} \tag{19}$$

In iteration $k+1$, the update formula for $u_{p,t}$ is as follows:

$$u_{p,t}^{(k+1)} = u_{p,t}^{(k,t)} + \sum_{i=1}^{NEV_p}P_{p,i,t}^{\mathrm{EVch},(k+1)} + \sum_{j=1}^{NBS_p}\left(P_{p,j,t}^{\mathrm{BSch},(k+1)} - P_{p,j,t}^{\mathrm{BSdis},(k+1)}\right) - P_{p,t}^{\mathrm{Grid},(k+1)} + P_{p,t}^{\mathrm{Load}} \tag{20}$$

In iteration $k+1$, the primal and dual residuals used to check convergence are

calculated as follows:

$$\begin{aligned}\left\|r_{p,t}^{k+1}\right\|_2 &= \left\|\sum_{i=1}^{NEV_p} P_{p,i,t}^{\mathrm{EVch},(k+1)} + \sum_{i=1}^{NBS_p}\left(P_{p,i,t}^{\mathrm{BSch},(k+1)} - P_{p,i,t}^{\mathrm{BSdis},(k+1)}\right) - P_{p,t}^{\mathrm{Grid},(k+1)} + P_{p,t}^{\mathrm{Load}}\right\|_2 \le \varepsilon^{pri} \\ \left\|s_{p,t}^{k+1}\right\|_2 &= \left\|\rho\left(\sum_{j=1}^{NBS_p}\left(P_{p,j,t}^{\mathrm{BSch},(k+1)} - P_{p,j,t}^{\mathrm{BSdis},(k+1)}\right) - P_{p,t}^{\mathrm{grid},(k+1)} - \left(\sum_{j=1}^{NBS_p}\left(P_{p,j,t}^{\mathrm{BSch},(k)} - P_{p,j,t}^{\mathrm{BSdis},(k)}\right) - P_{p,t}^{\mathrm{grid},(k)}\right)\right)\right\|_2 \le \varepsilon^{dual}\end{aligned} \tag{21}$$

After obtaining the optimal solution of the model, we can allocate incentive payments based on the contribution of EVs and BESS to mitigate the three-phase imbalance and peak-to-valley differences, according to Equations (22)-(24).

$$IB = PIB + TIB,\ IB^{\mathrm{EV}} = PIB^{\mathrm{EV}} + TIB^{\mathrm{EV}},\ IB^{\mathrm{BS}} = PIB^{\mathrm{BS}} + TIB^{\mathrm{BS}} \tag{22}$$

$$A = \frac{1}{\left(IB^{\mathrm{EV}} - IB\right)},\ B = \frac{1}{\left(IB^{\mathrm{BS}} - IB\right)} \tag{23}$$

$$EVreward = \frac{A}{A+B}\left(k^{Pib} PIB + k^{Tlb} TIB\right),\ BESSreward = \frac{B}{A+B}\left(k^{Pib} PIB + k^{Tlb} TIB\right) \tag{24}$$

PIB and TIB are calculated according to Equation (1). PIB^{EV} is the value of PIB when only the charging solutions of EVs are used to calculate PIB. TIB^{EV}, PIB^{BS} and TIB^{BS} have similar definitions to PIB^{EV}. Each EV owner acquires an equal share of the gross remuneration $EVreward$. The DSO acquires the remuneration of BESS $BESSreward$.

4. Stochastic Optimization Considering the Uncertainty of EV Charging

The deterministic model presented in Section 3 assumes that all plug-in EVs in the community will participate in the coordinating charging strategy and comply with the agreement, which is a bit idealistic. In practice, some EV users may be reluctant to participate in the scheme for commuting convenience or do not comply with the agreement after participating in the program. In this section, a scenario-based two-stage stochastic optimization model is proposed to cope with the load uncertainty caused by these EVs. Next, we will first describe the scenario generation and reduction methods, and then propose the model.

4.1 Uncertainty Scenario Generation and Reduction Methods

In this paper, a Monte Carlo simulation method is used to generate scenarios that reflect the uncertainty of EV charging. The uncertainty of EV charging is reflected in the uncertainty of EV arrival time and departure time at the charging station, and initial SoC level. Suppose that the DSO has the probability density functions for these three uncertainty parameters are $PDF_{arr}(t)$, $PDF_{dep}(t)$ and $PDF_{soc}(x)$. It is assumed that each EV starts charging on arrival and charges at rated power until fully charged or left. Then, the total charging power of all EVs at each moment can be calculated based on the arrival and departure times and the initial SoC level. Equation (25) is used to generate a certain number of scenarios that reflect the uncertainty of EV charging.

$$\begin{gathered}\sum_{t=1}^{T} PDF_{arr}(t)=1,\ \sum_{t=1}^{T} PDF_{dep}(t)=1,\ \sum_{x=1}^{100} PDF_{soc}(x)=1 \\ R_{i,arr}\in[0,1],\ R_{i,dep}\in[0,1],\ R_{i,soc}\in[0,1] \\ T_{i,arr}=arcPDF_{arr}(R_{i,arr}),\ T_{i,dep}=arcPDF_{dep}(R_{i,dep}),\ SOC_i=arcPDF_{dep}(R_{i,soc}) \\ T_{i,arr}<T_{i,dep}\end{gathered} \tag{25}$$

where $R_{i,arr}$, $R_{i,dep}$ and $R_{i,soc}$ are three random numbers that obey a uniform distribution on [0,1]; $T_{i,arr}$, $T_{i,dep}$ and SoC_i are the arrival time, departure time, and initial SoC level of EV i in one of the scenarios generated by the simulation, respectively.

If there are NOP EVs on the grid that do not participate in the coordinated charging strategy presented in Section 3, then the grid needs to consider the uncertainty of these EV charging. By sampling the arrival and departure times and the initial SoC level of these EVs, according to Equation (25), then, the total charging load required by these EVs on each phase at each moment can be calculated based on the second

assumption above. An example of a scenario is given in Equation (26).

$$\omega_k = \left(P_{0,1}^{\mathrm{EVch},k}, P_{0,2}^{\mathrm{EVch},k}, P_{0,3}^{\mathrm{EVch},k}, P_{1,1}^{\mathrm{EVch},k}, P_{1,2}^{\mathrm{EVch},k}, P_{1,3}^{\mathrm{EVch},k}, ..., P_{T,1}^{\mathrm{EVch},k}, P_{T,2}^{\mathrm{EVch},k}, P_{T,3}^{\mathrm{EVch},k} \right) \quad (26)$$

For an optimization problem, if the number of scenarios is too large, it will increase the computational complexity. If the number of scenarios is too small, the accuracy of simulation results will not be high. To overcome this difficulty, we use the scenario reduction method based on probability metrics to eliminate scenarios with small probability and collect similar scenarios. Simultaneous Backward Reduction is used in this paper, the detailed processes are shown below:

1) Suppose that we have obtained Nk scenarios ω_k, each with an occurrence probability of $p_k = \frac{1}{Nk}$; we expect to reduce the number of scenarios to NR. We set up two sets, a set S that holds the initial scenarios and an empty set D that is used to hold the scenarios to be eliminated later. Calculate the distance $D(\omega_x, \omega_y)$ between each pair of scenarios in S, according to Equation (27)

$$D(\omega_x, \omega_y) = \sqrt{\sum_{p=1}^{3} \sum_{t=0}^{T} (\lambda_{t,p}^{x} - \lambda_{t,p}^{y})^2} \quad (27)$$

2) For each scenario k in S, find the scenario r that has the shortest distance from scenario k, according to Equation (28).

$$d(\omega_k, \omega_r) = \min_s \{ D(\omega_k, \omega_s), s \in S, k \neq s \}, k \in S, \quad (28)$$

3) After finding the shortest distance scenario r for each scenario $k \in S$, calculate $Pd_k(r)$ according to $Pd_k(r) = p_k * d(\omega_k, \omega_r)$. Find the scenario d that has the smallest value of $Pd_k(r)$, according to $Pd_d = \min_k Pd_k(r), k \in S$.

4) Eliminate scenario d, and update sets S and D, according to

$S = S - \{d\}$, $DS = DS + \{d\}$. Recalculate the probability of scenario r that has the shortest distance from scenario d, according to $p_r = p_r + p_d$.

5) Repeat steps 2)-4) until the total number of remaining scenarios is NR.

4.2 Scenario-based Two-stage Stochastic Optimization Model

In this section, a scenario-based two-stage stochastic optimization model is proposed to cope with the load uncertainty caused by these EVs. The first stage decision is made before uncertainty is known and the second stage decision is made after uncertainty is observed. The first stage simulates the day-ahead operation plan of the grid, and the second stage simulates the real-time operation. In the first stage, in addition to optimizing the charging and discharging strategies for those EVs and BESS participating in the energy management program, the grid's power reserve allocation strategy will be optimized to ensure that sufficient reserves can be provided for the second stage to cope with the load uncertainty caused by those EVs not participating in the coordinated charging strategy. In the second stage, the power provided by the grid and the charging and discharging power of the BESS are adjusted to deal with each of the uncertain scenarios obtained above, based on the optimization results of the first stage. The power adjustment for each scenario is less than the reserve provided in the first stage. The mathematical formulation of the proposed scenario-based two-stage stochastic optimization model is shown in Equations (29)-(53).

$$\begin{aligned}\min\ & k^{\mathrm{Pib}}\sum_{t=1}^{T}\sum_{p=1}^{3}\left(P_{p,t}^{\mathrm{Grid}}-\frac{1}{3}\sum_{p=1}^{3}P_{p,t}^{\mathrm{Grid}}\right)^2+k^{\mathrm{Tib}}\sum_{t=1}^{T}\sum_{p=1}^{3}\left(P_{p,t}^{\mathrm{Grid}}-\frac{1}{T}\sum_{t=1}^{T}P_{p,t}^{\mathrm{Grid}}\right)^2\\&+\sum_{t=1}^{T}\sum_{p=1}^{3}\sum_{i=1}^{NEV_p}p_t^{\mathrm{Price}}P_{p,i,t}^{\mathrm{EVch}}\Delta t\\&+\sum_{t=1}^{T}\sum_{p=1}^{3}\sum_{j=1}^{NBS_p}p_t^{\mathrm{Price}}\left(P_{p,j,t}^{\mathrm{BSch}}-P_{p,j,t}^{\mathrm{BSdis}}\right)\Delta t\\&+0.5\times\sum_{t=1}^{T}\sum_{p=1}^{3}\sum_{j=1}^{NBS_p}\frac{\left|\eta_{p,j}^{\mathrm{BSch}}P_{p,j.t}^{\mathrm{BSch}}-P_{p,j,t}^{\mathrm{BSdis}}/\eta_{p,j}^{\mathrm{BSdis}}\right|\times\Delta t}{\mathrm{L}_{cyc}^{80\%}}\times p_{bat}^{\mathrm{Price}}\\&+k^{\mathrm{RG}}\sum_{t=1}^{T}\sum_{p=1}^{3}\left(R_{p,t}^{\mathrm{GridU}}+R_{p,t}^{\mathrm{GridD}}\right)+k^{\mathrm{RB}}\sum_{t=1}^{T}\sum_{p=1}^{3}\sum_{j=1}^{NBS_p}\left(R_{p,j,t}^{\mathrm{BSchU}}+R_{p,j,t}^{\mathrm{BSchD}}+R_{p,j,t}^{\mathrm{BSdisU}}+R_{p,j,t}^{\mathrm{BSdisD}}\right)\end{aligned}\tag{29}$$

Constraints (3), (5)-(9), (12)-(17)

$$P_{p,t}^{\mathrm{Grid}}+R_{p,t}^{\mathrm{GridU}}\le P_p^{\mathrm{GridMax}},\ \forall p,\forall t\tag{30}$$

$$P_{p,t}^{\mathrm{Grid}}-R_{p,t}^{\mathrm{GridD}}\ge 0,\ \forall p,\forall t\tag{31}$$

$$R_{p,t}^{\mathrm{GridU}},R_{p,t}^{\mathrm{GridD}}\ge 0\tag{32}$$

$$0\le P_{p,j,t}^{\mathrm{BSch}}+R_{p,j,t}^{\mathrm{BSchU}}\le y_{p,j,t}^{\mathrm{BSch}}\cdot P_{p,j}^{\mathrm{BSmax}},\ \forall p,\forall j,\forall t\tag{33}$$

$$0\le P_{p,j,t}^{\mathrm{BSch}}-R_{p,j,t}^{\mathrm{BSchD}},\ \forall p,\forall j,\forall t\tag{34}$$

$$0\le P_{p,j,t}^{\mathrm{BSdis}}+R_{p,j,t}^{\mathrm{BSdisU}}\le y_{p,j,t}^{\mathrm{BSdis}}\cdot P_{p,j}^{\mathrm{BSmax}},\ \forall p,\forall j,\forall t\tag{35}$$

$$0\le P_{p,j,t}^{\mathrm{BSdis}}-R_{p,j,t}^{\mathrm{BSdisD}},\ \forall p,\forall j,\forall t\tag{36}$$

$$E_{p,j,t}^{\mathrm{BS}}+R_{p,j,t}^{\mathrm{BSchU}}\cdot\eta_{p,j}^{\mathrm{BSch}}\cdot\Delta t\le E_{p,j}^{\mathrm{BSmax}},\ \forall p,\forall j,\forall t\tag{37}$$

$$E_{p,j}^{\mathrm{BSmin}}\le E_{p,j,t}^{\mathrm{BS}}-\frac{R_{p,j,t}^{\mathrm{BSdisU}}\cdot\Delta t}{\eta_{p,j}^{\mathrm{BSdis}}},\ \forall p,\forall j,\forall t\tag{38}$$

$$R_{p,j,t}^{\mathrm{BSchU}},R_{p,j,t}^{\mathrm{BSchD}},R_{p,j,t}^{\mathrm{BSdisU}},R_{p,j,t}^{\mathrm{BSdisD}}\ge 0,\ \forall p,\forall j,\forall t\tag{39}$$

where $R_{p,t}^{\mathrm{GridU}}$, $R_{p,t}^{\mathrm{GridD}}$, $R_{p,j,t}^{\mathrm{BSchU}}$, $R_{p,j,t}^{\mathrm{BSch,D}}$, $R_{p,j,t}^{\mathrm{BSdisU}}$, and $R_{p,j,t}^{\mathrm{BSdisD}}$ are up-spinning and down-spinning reserve provided by the grid and BESS, respectively. Constraints (30)-(32) are used to ensure the power flow limits of the distribution feeders. Constraints (33)-(39) are operating limits of BESS, including charging and discharging power limits, energy capacity.

In the second stage, the scenarios generated by methods shown in Section 4.1 are

used. The uncertainty of EV charging mathematically makes $P_{p,t}^{\text{Load}}$ an uncertain parameter in the optimization model. By adding the EV charging load in each scenario to the original uncontrollable load in the community, we can obtain the total load in each scenario $P_{p,t,s}^{\text{Load}}$. Therefore, the constraints for the second stage are shown as follows:

$$P_{p,t,s}^{\text{GridReal}}=P_{p,t,s}^{\text{Load}}+\sum_{i=1}^{NEV_p}P_{p,i,t}^{\text{EVch}}+\sum_{j=1}^{NBS_p}\left(P_{p,j,t,s}^{\text{BSchReal}}-P_{p,j,t,s}^{\text{BSdisReal}}\right),\ \forall p,\forall t,\forall s \tag{40}$$

$$P_{p,t,s}^{\text{GridReal}}=P_{p,t,s}^{\text{Grid}}+R_{p,t,s}^{\text{GridRealU}}-R_{p,t,s}^{\text{GridRealD}} \tag{41}$$

$$0\le R_{p,t,s}^{\text{GridRealU}}\le R_{p,t}^{\text{GridU}},\ \forall p,\forall t,\forall s \tag{42}$$

$$0\le R_{p,t,s}^{\text{GridRealD}}\le R_{p,t}^{\text{GridD}},\ \forall p,\forall t,\forall s \tag{43}$$

$$P_{p,j,t,s}^{\text{BSchReal}}=P_{p,j,t}^{\text{BSch}}+R_{p,j,t,s}^{\text{BSchRealU}}-R_{p,j,t,s}^{\text{BSchRealD}},\ \forall p,\forall j,\forall t,\forall s \tag{44}$$

$$P_{p,j,t,s}^{\text{BSdisReal}}=P_{p,j,t}^{\text{BSdis}}+R_{p,j,t,s}^{\text{BSdisRealU}}-R_{p,j,t,s}^{\text{BSdisRealD}},\ \forall p,\forall j,\forall t,\forall s \tag{45}$$

$$0\le P_{p,j,t,s}^{\text{BSchReal}}\le y_{p,j,t}^{\text{BSch}}\cdot P_{p,j}^{\text{BSmax}},\ \forall p,\forall j,\forall t,\forall s \tag{46}$$

$$0\le P_{p,j,t,s}^{\text{BSdisReal}}\le y_{p,j,t}^{\text{BSdis}}\cdot P_{p,j}^{\text{BSmax}},\ \forall p,\forall j,\forall t,\forall s \tag{47}$$

$$0\le R_{p,j,t,s}^{\text{BSchRealU}}\le R_{p,j,t}^{\text{BSchU}},\ \forall p,\forall j,\forall t,\forall s \tag{48}$$

$$0\le R_{p,j,t,s}^{\text{BSchRealD}}\le R_{p,j,t}^{\text{BSchD}},\ \forall p,\forall j,\forall t,\forall s \tag{49}$$

$$0\le R_{p,j,t,s}^{\text{BSdisRealU}}\le R_{p,j,t}^{\text{BSdisU}},\ \forall p,\forall j,\forall t,\forall s \tag{50}$$

$$0\le R_{p,j,t,s}^{\text{BSdisRealD}}\le R_{p,j,t}^{\text{BSdisD}},\ \forall p,\forall j,\forall t,\forall s \tag{51}$$

$$E_{p,j,t,s}^{\text{BSReal}}-E_{p,j,t-1,s}^{\text{BSReal}}-\Delta t\cdot\eta_{p,j}^{\text{BSchReal}}\cdot P_{p,j,t,s}^{\text{BSchReal}}+\Delta t\cdot\frac{P_{p,j,t,s}^{\text{BSdisReal}}}{\eta_{p,j}^{\text{BSdis}}}=0,\ \forall p,\forall j,\forall t,\forall s \tag{52}$$

$$E_{p,j}^{\text{BSmin}}\le E_{p,j,t,s}^{\text{BSReal}}\le E_{p,j}^{\text{BSmax}},\ \forall p,\forall j,\forall t,\forall s \tag{53}$$

where $P_{p,t,s}^{\text{GridReal}}$, $P_{p,j,t,s}^{\text{BSchReal}}$ $P_{p,j,t,s}^{\text{BSdisReal}}$ are power provided by the grid, charging and discharging power of BESS in the real-time stage. $R_{p,t,s}^{\text{GridRealU}}$, $R_{p,t,s}^{\text{GridRealD}}$, $R_{p,j,t,s}^{\text{BSchRealU}}$, $R_{p,j,t,s}^{\text{BSchRealD}}$, $R_{p,j,t,s}^{\text{BSdisRealU}}$, and $R_{p,j,t,s}^{\text{BSdisRealD}}$ are up-power or down-power adjustments from the grid and

BESS in the real-time stage, respectively. They must be smaller than the up-spinning and down-spinning reserve provided by the grid and BESS. Constraints (42)-(43) are power adjustment limits of the grid. Constraints (48)-(51) are charging and discharging power adjustment and energy capacity limits of BESS.

With the above model, we can get a coordinated charging and discharging strategy for EVs and BESS that reduces the three-phase power imbalance and peak-to-valley difference, and a reserve scheme that can cope with the uncertainty of the load.

5. Numerical Results

To verify the effectiveness and efficiency of the proposed energy management scheme and distributed optimization algorithm for EVs and BESSs, the IEEE 34-node test feeder [22] as shown in Fig. 4(a) is modified for numerical simulation. In the deterministic model, it is assumed that:

（1） Node 890 (marked in red in Fig. 4(a)) is chosen to serve as the three-phase distribution system described in Section 2.1. There are 300 EV chargers and a BESS connected to each phase of node 890.

（2） All EVs are willing to participate in the proposed energy management scheme. The maximum charging rate of each EV is fixed at 2.3 kW and the battery capacity is 17 kWh [23].

（3） As for BESS, the maximum charging and discharging rate are fixed at 60 kW and the battery capacity is 60 kWh. The initial SoC of the BESS is 60%. The minimum and maximum SoC of the BESS are 20% and 100%, respectively. $L_{cyc}^{80\%}$ and p_{bat}^{Price} are set to be 10000 and 150, respectively. The charging and discharging efficiency of EVs and

BESS is 97.46% [24].

We consider an optimization period of 8 hours from 9:00 to 16:00 in hourly intervals. The price for each time slot is shown in Fig. 4 (b). In the objective function, k^{Pib} and k^{Tib} are set as 0.01. In the distribution algorithm, the value of ρ, ε^{primal} and ε^{dual} are set to be 0.1, 0,01, and 0.01, respectively. Based on the above parameters, various case studies are conducted to demonstrate the effectiveness of the proposed model in mitigating three-phase imbalance and peak-to-valley differences. We expect that loss costs will be reduced as well as improving the power quality. The proposed optimization model is programmed on MATLAB 2020b platform with Yalmip toolbox and solved by Gurobi 9.1.2.

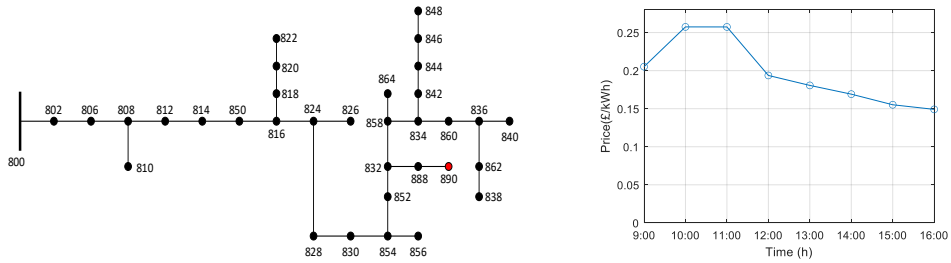

(a) (b)

Fig. 4. (a) Topology of the IEEE 34-node test feeder; (b) Time-of-use electricity price.

5.1 Effectiveness in Mitigating Phase Imbalance and Peak-to-valley Differences

In this subsection, the effectiveness of the proposed model for reducing the three-phase power imbalance and peak-to-valley differences is investigated. Fig. 5(a) shows the active power consumption of the uncontrollable load. The figure shows that the uncontrollable load of the three phases is unbalanced. This imbalance may be aggravated by the random charging behavior of EVs. Fig. 5(b) shows an example of the active power consumption generated by the random charging behavior of the EVs, which is generated by randomly sampling the initial SoC level, arrival, and departure times of the EVs. The

total active power consumption of the three-phase distribution feeder obtained from the uncontrollable load and the EV is shown in Fig. 5(c). The results in Fig. 5(c) show that the power imbalance between the three phases increases at certain times of the day due to the random charging of EVs. The peak-to-valley difference of the load curve also increases. The proposed optimization models described in Sections 2 and 3 are used to optimize the charging and discharging strategies of EVs and BESS. The purpose is to reduce 1. The random charging behavior of EVs aggravating the phase imbalance; 2. phase imbalance caused by uncontrollable loads.

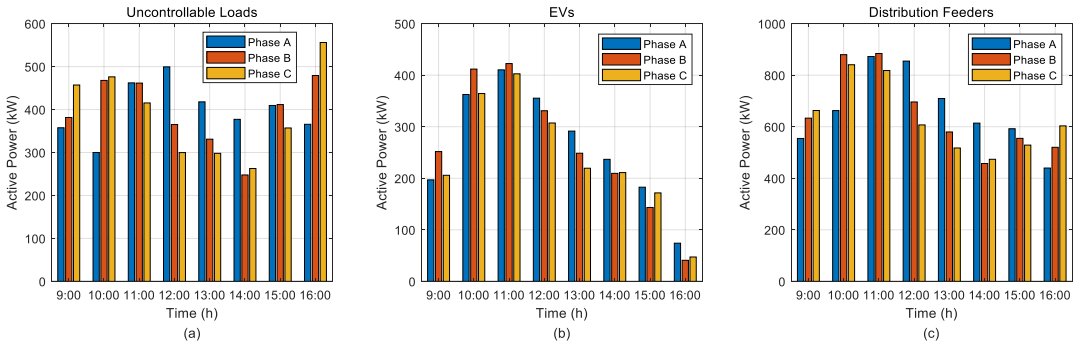

Fig. 5. Active power consumption of (a) the uncontrollable loads; (b) EVs; (c) distribution feeders before coordinated optimization.

Fig. 6(a) shows the optimal active power consumption for EV charging. Note that the initial and final SoC of EVs is the same as in Fig. 5(b). Fig. 6(b) shows the optimal charging and discharging power and SoC of the BESS. The total active power flow on the distribution feeder is shown in Fig. 6(c). Fig. 6(c) shows that the imbalance of the three-phase active power flow on the distribution feeder is greatly reduced compared to Fig. 5(c). Figs. 6 (b) and 6 (c) show that the EV and BESS will charge and discharge according to the three-phase power imbalance level of the uncontrollable load. For example, as shown in Fig. 5(a) at 9:00, phase C has the heaviest active power consumption of uncontrollable load, so the EVs in phase C decrease charging while the BESS in phase C

increases discharging. Conversely, phase A has the lightest active power consumption of uncontrollable load, so the EV in phase A increases charging while the BESS decreases discharging. Fig. 6(c) also shows that the power imbalance at different time slots is also reduced, i.e., the peak-to-valley difference of the load curve is reduced. For quantitative analysis, according to Equation (1), we can also calculate the *PIB* which reflects the variance of the power flow for the three phases, and *TIB* which reflects the variance of the power flow for different time slots in the time horizon. According to Figs. 5(c) and 6(c), we can also obtain the maximum power consumption *MAP* and the minimum power consumption *MIP* on each phase before and after optimization. The results are shown in Table 1. *PIB*, *TIB* and *MAP* are significantly reduced after optimization while the *MIP* increases. The maximum power consumption is reduced from 884.2 kW to 699.3 kW. The minimum power consumption increases from 439.8 kW to 576.9 kW. Therefore, the simulation results discussed above indicate that the proposed model can mitigate the imbalance of active power consumption on the three phases and reduce the peak-to-valley difference of each phase. These are achieved by optimizing the charging and discharging power and time of EVs and BESS.

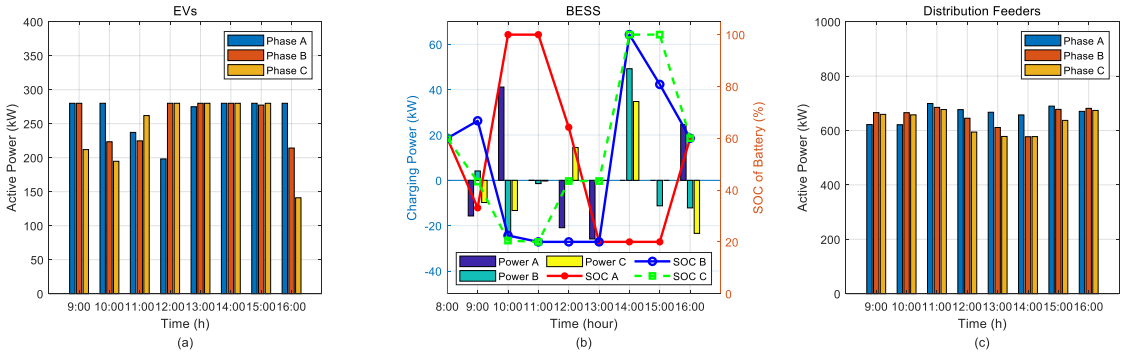

Fig. 6. Active power consumption of (a) EVs; (b) BESS; (c) distribution feeder after coordinated optimization.

Table 1. The phase imbalance and power imbalance index before and after optimization.

Index	*PIB* (kW^2)	*TIB* (kW^2)	*MAP* (kW)	*MIP* (kW)
Before Optimization	116451.1	459150.1	884.2	439.8
After Optimization	15821.7	28555.8	699.3	576.9

5.2 Power Quality and Economic Effects

In this subsection, we investigate the impact of the proposed scheme on the power quality and operating cost of the IEEE 34-node test feeder. To perform the above analysis, a three-phase power flow calculation is performed. After obtaining the optimal charging and discharging power of the EV and BESS at node 890, we calculate the reactive power consumption of node 890 based on the power factor of 0.95. The active and reactive power consumption at node 890 before the optimization is shown in Table 2. The active and reactive power consumption at node 890 after the optimization is shown in Table 3. The active and reactive power consumption of other nodes is shown in Table 4. With the active and reactive power consumption data, as shown in Tables 2-4, and the impedance matrix of the distribution lines, we can calculate the voltage value of each bus in the system and the current of each line to analyze the power quality, where the line impedance matrix can be calculated based on the methodology presented in [25] and the data in [22].

Table 2. The active and reactive power consumption at node 890 before optimization

Time	Phase A		Phase B		Phase C	
(Hour)	kW	kVAr	kW	kVAr	kW	kVAr
9:00	554.5	182.2	633.2	208.1	662.9	217.8
10:00	662.6	217.7	879.6	289.1	840.5	276.2
11:00	872.4	286.7	884.2	290.5	818.1	268.8
12:00	854.7	280.9	696.1	228.7	607.0	199.5
13:00	709.4	233.1	579.6	190.5	517.5	170.0
14:00	614.0	201.8	457.2	150.2	473.7	155.6
15:00	592.2	194.6	554.9	182.3	528.7	173.7
16:00	439.8	144.5	520.1	170.9	603.3	198.2

Table 3. The active and reactive power consumption at node 890 after optimization

Time	Phase A		Phase B		Phase C	
(Hour)	kW	kVAr	kW	kVAr	kW	kVAr
9:00	621.8	204.4	665.4	218.7	659.2	216.6
10:00	621.2	204.1	665.2	218.6	657.4	216.1
11:00	699.3	229.9	684.7	225.0	677.0	222.5
12:00	673.9	221.5	645.0	212.0	579.8	190.5
13:00	669.4	220.0	611.0	200.8	589.4	193.7
14:00	657.2	216.0	576.9	189.6	580.5	190.8
15:00	689.5	226.6	677.8	222.8	637.1	209.4
16:00	670.3	220.3	681.5	224.0	673.8	221.4

Table 4. Active and reactive power consumption of the uncontrollable loads at other nodes (non-zero elements)

Phases	Phase A		Phase B		Phase C	
Nodes	kW	kVAr	kW	kVAr	kW	kVAr
860	20	16	20	16	20	16
840	9	7	9	7	9	7
844	135	105	135	105	135	105
848	20	16	20	16	20	16
830	10	5	10	5	10	5

After obtaining the voltage amplitude and line current, we calculate the voltage imbalance at each node and the current imbalance of each line segment with Equation (54). The neutral current in a line segment can be calculated with Equation (20) in [25].

$$\begin{aligned} VIB &= \frac{Max\left(\left|V_A - V_{avg}\right|, \left|V_B - V_{avg}\right|, \left|V_C - V_{avg}\right|\right)}{V_{avg}}, \; V_{avg} = \frac{V_A + V_B + V_C}{3} \\ IIB &= \frac{Max\left(\left|I_A - I_{avg}\right|, \left|I_B - I_{avg}\right|, \left|I_C - I_{avg}\right|\right)}{I_{avg}}, \; I_{avg} = \frac{I_A + I_B + I_C}{3} \end{aligned} \tag{54}$$

The voltage imbalance of node 890, current imbalance and neutral current of line segment 800-802 are shown in Figs. 7(a), 7(b) and 7(c). The figure shows that after optimizing the charging and discharging strategies for EVs and BESS, not only the voltage magnitude and line current imbalance are mitigated but also the current in the neutral line is reduced. This confirms that the power quality of the distribution system has

improved.

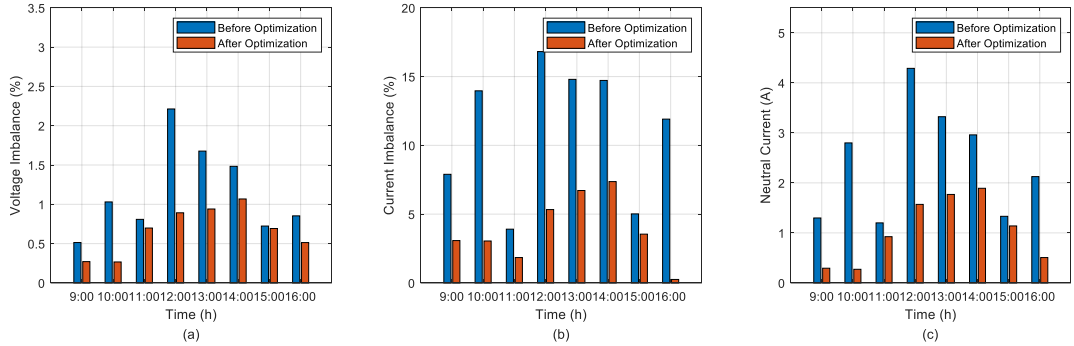

Fig. 7. (a) Voltage imbalance at node 890; (b) Current imbalance of line segment 800-802; (c) Neutral currents in line segment 800-802

In the following section, we will discuss the economic effects contributed by the proposed model. Based on Equation (24), we can calculate the incentive revenue that EVs and BESS receive from the DSO. The final charging cost of the EVs and BESS can be obtained by subtracting the incentive revenue from the charging cost of the EVs, as shown in (55).

$$C_{EV} = \sum_{t=1}^{T}\sum_{p=1}^{3}\sum_{i=1}^{NEV_p} p_t^{\text{Price}} P_{p,i,t}^{\text{EVch}} \Delta t - EVreward$$

$$C_{BESS} = \sum_{t=1}^{T}\sum_{p=1}^{3}\sum_{j=1}^{NBS_p} p_t^{\text{Price}} \left(P_{p,j,t}^{\text{BSch}} - P_{p,j,t}^{\text{BSdis}}\right)\Delta t \tag{55}$$

$$+0.5\times\sum_{t=1}^{T}\sum_{p=1}^{3}\sum_{j=1}^{NBS_p} \frac{\left|\eta_{p,j}^{\text{BSch}} P_{p,j.t}^{\text{BSch}} - P_{p,j,t}^{\text{BSdis}} / \eta_{p,j}^{\text{BSdis}}\right|\times\Delta t}{\text{L}_{cyc}^{80\%}} \times p_{bat}^{\text{Price}} - BESSreward$$

The operation cost of the DSO is defined as the remuneration provided to the EV and BESS pluses the energy loss cost. The energy losses of the three-phase distribution system are calculated according to the method proposed in [25].

$$C_{DSO,before} = \sum_{t=1}^{T}\sum_{p=1}^{3} p_t^{\text{Price}} P_{p,t}^{Loss} \Delta t$$

$$C_{DSO,after} = \sum_{t=1}^{T}\sum_{p=1}^{3} p_t^{\text{Price}} P_{p,t}^{Loss} \Delta t + EVreward + BESSreward \tag{56}$$

$$C_{DSO,increased} = C_{DSO,after} - C_{DSO,before}$$

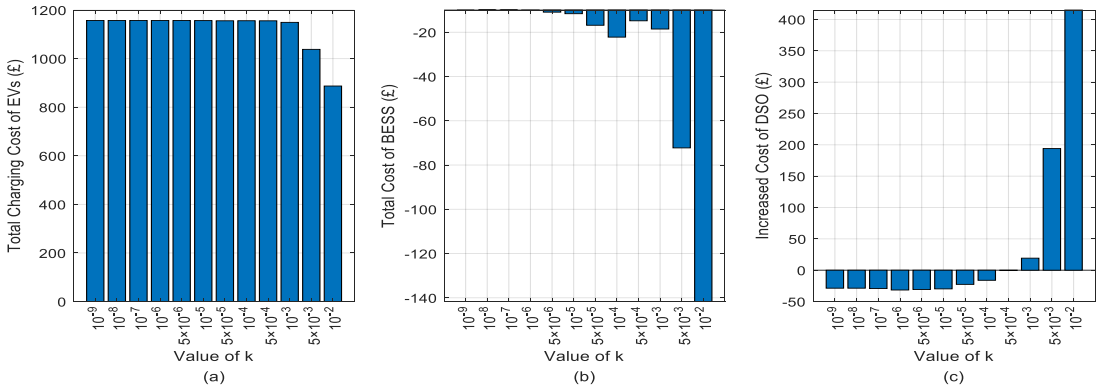

Fig. 8. (a) The final charging cost of EVs; (b) BESS; (c) DSO when the value of k varies.

Figs. 8(a) and 8(b) show the total charging cost of EVs C_{EV}, the total cost of BESS C_{BESS} when the value of k $\left(k = k^{Pib} = k^{Tib}\right)$ varies. Fig. 8(c) shows the increased operation cost $C_{DSO,increased}$ of the DSO after the optimization. In Fig. 8(a), we can see that the cost of EVs is decreased as k increases due to the payoffs have already been included. EVs make some sacrifices in charging flexibility to help the DSO reduce phase and power imbalances and in return, EVs get paid to reduce their costs. As shown in Fig. 8(b), the BESS has a negative value of C_{BESS}, which means BESS is also making a profit. As for DSO, it benefits from reduced energy losses and investment costs, as well as improved power quality due to reduced phase imbalances and peak-to-valley differences. As shown in Fig. 8(c), the negative value of $C_{DSO,increased}$ implies that the DSO can be profitable by reducing energy losses. Fig. 9(b) shows the total energy loss of the distribution system as the value of k varies. We can see that as k increases, the expected total energy loss of this distribution system decreases. The operating cost of the DSO also decreases as the energy loss decreases, as shown in Fig. 8(c). Note that the total energy loss no longer changes when k increases to a certain value. This is because the power imbalance index has no more change, as shown in Fig. 9(a). However, according to Equations (24) and (55), the DSO pays more to EVs and BESS as k increases. Thus, by changing the value

of k, the DSO can control the charging and discharging behavior of the EVs and BESS. The DSO can choose an appropriate value of k for its benefits.

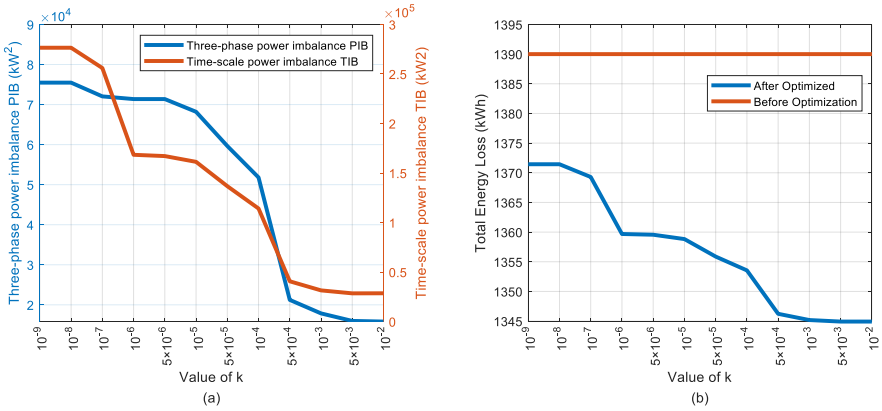

Fig. 9. (a) The phase imbalance and power imbalance of the system; (b) Total energy loss in the system when the value of k varies.

As for the convergence speed of the proposed distributed optimization approach, Fig. 10 shows the maximum primal and dual residuals in each iteration. The figure shows that the algorithm converges after 63 iterations and the total simulation time is 216.75s. Therefore, our proposed algorithm can converge with an acceptable time practically.

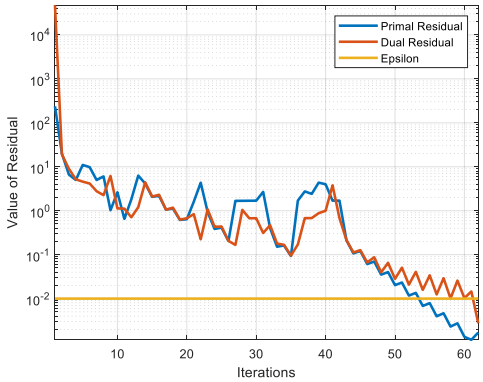

Fig. 10. Convergence curve of the distributed algorithm: the maximum primal and dual residuals.

5.3 Effectiveness of The Proposed Stochastic Optimization Model to Cope with The Uncertainty of EVs

In this section, we investigate the scenario generation and reduction approach and the scenario-based two-stage stochastic optimization model proposed in Section 4 to verify its effectiveness in dealing with the uncertainty of EVs. The probability density

functions of EV arrival time, departure time, and initial SoC level shown in Fig. 11 were used in the simulation. In this paper, 200 uncertainty scenarios were generated and reduced to 40 using the scenario generation and reduction methods presented in Section 4.1. These 40 scenarios are considered in the proposed stochastic optimization model to get an optimal reserve schedule.

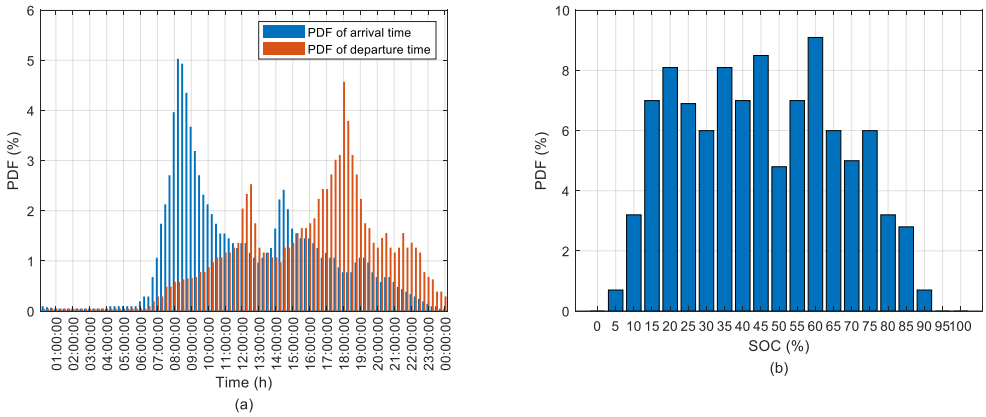

Fig. 11. The probability density functions of (a) EV arrival time, departure time, and (b) initial SoC level.

Figs. 12(a) and 12(b) show the optimal power flow in the three-phase distribution feeders of the optimization model with and without uncertainty scenario constraints, respectively. Table 5 demonstrates the phase imbalance and power imbalance index of the optimization models with and without scenario constraints. The definition of all indexes can be found in Section 5.1. Fig. 13(a) and 13(b) show optimal up-spinning and down-spinning reserves provided by grid and BESS for the optimization model with uncertainty scenario constraints.

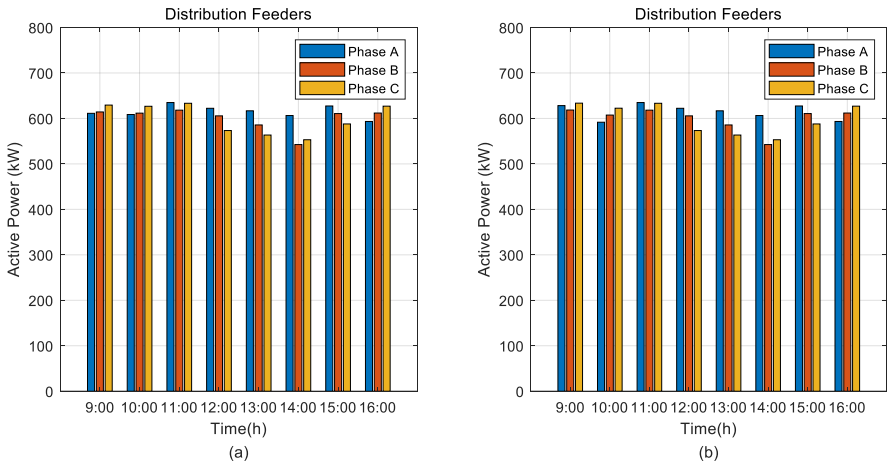

Fig. 12. Power flow in the three-phase distribution feeders of the optimization model (a) without and (b) with uncertainty scenarios.

Table 5. The phase imbalance and power imbalance index of the optimization models with and without scenario constraints.

Index	*PIB* (kW^2)	*TIB* (kW^2)	*MAP* (kW)	*MIP* (kW)
Without Scenarios	6913.9	13468.2	634.9	542.5
With Scenarios	7129.3	14247.1	634.9	542.5

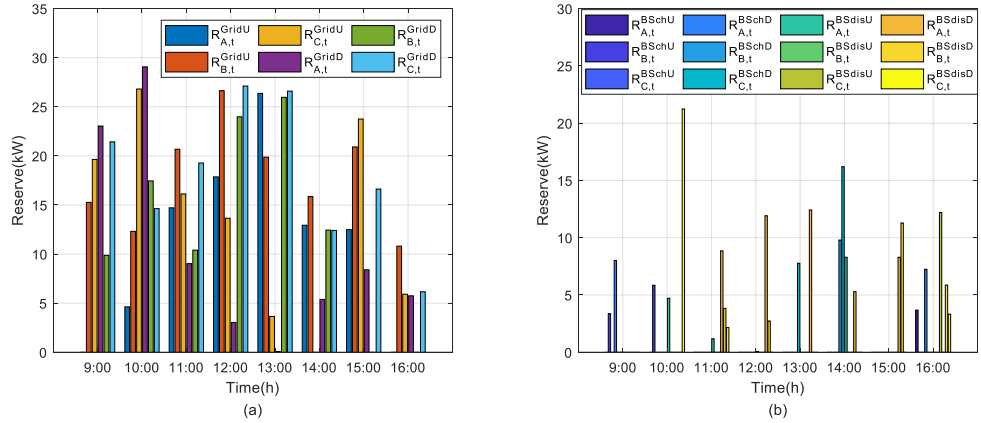

Fig. 13. Up-spinning and down-spinning reserve provided by (a) grid and (b) BESS.

It can be seen from Fig. 12(a) that the three-phase power of the proposed stochastic optimization model is generally balanced. However, as seen in Table 5, the three-phase power imbalance level (*PIB*) and the variance of the power flow for different time slots of all phases (*TIB*) of the optimization model with uncertainty scenario constraint is a bit higher than that of the optimization model without uncertainty scenario constraint. This is reasonable, because the more constraints there are, the larger the value of the objective function will be. Although the three-phase power balance of the optimization model with

uncertainty scenario constraints is slightly reduced, a reserve schedule that can cope with load uncertainty can be obtained in this model, as shown in Fig. 13.

To investigate the effectiveness of the reserve schedule to cope with the uncertainty of EV charging, we designed a feasible check subproblem as shown in Equations (57)-(59) below.

$$S = \min \sum_{p=1}^{3} \sum_{t=1}^{T} \left(S1_{p,t,s} + S2_{p,t,s} \right) \tag{57}$$

$$P_{p,t,s}^{\text{GridReal}} + S1_{p,t,s} - S2_{p,t,s} = P_{p,t,s}^{\text{Load}} + \sum_{i=1}^{NEV_p} P_{p,i,t}^{\text{EVch}} + \sum_{j=1}^{NBS_p} \left(P_{p,j,t,s}^{\text{BSchReal}} - P_{p,j,t,s}^{\text{BSdisReal}} \right) - PV_{p,t}, \ \forall p, \forall t, \forall s \tag{58}$$

$$S1_{p,t,s} \geq 0, S2_{p,t,s} \geq 0, \forall p, \forall t, \forall s \tag{59}$$

Constraints: (41)-(53)

In (42)-(43) and (44)-(51) the value of $P_{p,t,s}^{\text{Grid}}$, $P_{p,j,t}^{\text{BSch}}$, $P_{p,j,t}^{\text{BSdis}}$, $R_{p,t}^{\text{GridU}}$, $R_{p,t}^{\text{GridD}}$, $R_{p,j,t}^{\text{BSchU}}$, $R_{p,j,t}^{\text{BSch,D}}$, $R_{p,j,t}^{\text{BSdisU}}$, $R_{p,j,t}^{\text{BSdisD}}$, $y_{p,j,t}^{\text{BSch}}$ and $y_{p,j,t}^{\text{BSdis}}$ are the optimal results of the stochastic optimization model.

We tested the feasibility of 200 scenarios with different $P_{p,t,s}^{\text{Load}}$. In some scenarios, if the optimization objective S of the feasibility problem is equal to zero, it means that there is no violation and the reserve schedule can handle this scenario. Otherwise, it means that the reserve schedule cannot maintain the power balance of the real-time state. For comparison, we also tested the two cases of 20% reduction and 20% increase in reserve, which can be considered as low and high reserve states, keeping the remaining parameters constant. The results of feasibility checks for different reserve schedules are shown in Table 6.

Table 6. Results of feasibility checks for different reserve schedules

The objective value of the feasibility check subproblem	Optimal reserve schedule	20% reduction in reserve	20% increase in reserve
Number of scenarios S =0	89	18	119
Number of scenarios $S > 0$	111	182	81

As can be seen from Table 6, even in the optimal reserve schedule, the objective value of the feasibility check subproblem in some cases is greater than zero. This is reasonable because the stochastic optimization model cannot take all the uncertainties into account considering the reserve cost and the problem size. In this paper, 40 out of 200 scenarios are selected for optimization and there is no guarantee that all scenarios other than these 40 will be satisfied. However, we can see that the optimal reserve schedule obtained from the proposed two-stage scenario-based optimization model can handle 89 out of 200 scenarios. This means that the optimal reserve scheme keeps the real-time power balanced not only for these 40 scenarios but also for the other 49 scenarios. This proves that the scenario reduction method used in this paper is effective and representative scenarios can be selected.

As for the other two reserve schedules, when the reserve decreases by 20%, only 18 scenarios can be handled and 182 scenarios violate the power balance constraint. When the reserve is increased by 20%, 119 scenarios can be handled, which is only 20 more than the optimal reserve schedule. The fewer reserves the system has, the less reliable the system will be, however, the more reserves, the higher the cost. Therefore, by comparing the above two reserve schedules, it can be seen that the proposed model can obtain a more economical and relatively reliable reserve schedule.

In summary, with the proposed scenario-based two-stage stochastic optimization

model, we can obtain a coordinated charging and discharging strategy for EVs and BESSs that can reduce three-phase power imbalance and peak-to-valley differences, as well as a reserve scheme that can cope with load uncertainty to some extent.

6. Conclusions

This paper presents a phase-balancing and peak-shaving energy management scheme for the three-phase distribution system, by optimizing the charging and discharging strategies for EVs and grid BESS. Both centralized and distributed optimization models are examined. Simulation results demonstrate that the phase imbalance and peak-to-valley differences of the three-phase load curve are reduced after the optimization. The total energy loss of the distribution system is reduced and power quality is improved with the mitigation of voltage imbalance and current in the neutral line. Both EVs and DSO benefit from the scheme. For future work, we will consider power flow constraints based on the three-phase power flow model to make the model more suitable for large-scale power distribution systems. Reactive power management can also be considered.

Acknowledgment

This work is sponsored by Brunel University London BRIEF Funding; the Department of Finance and Education of Guangdong Province 2016 [202]: Key Discipline Construction Program, China; Education Department of Guangdong Province: New and Integrated Energy System Theory and Technology Research Group [Project Number 2016KCXTD022]. We are grateful for support from the DTE Network+ funded by EPSRC grant reference EP/S032053/1.

Reference

[1]. R. M. Ciric, et al., Power flow in four-wire distribution networks-general approach, IEEE Trans. Power Syst. 18(4) (2003) 1283-1290.

[2]. K. Ma, et al., Review of distribution network phase unbalance: Scale, causes, consequences, solutions, and future research directions, CSEE Journal of Power and Energy Systems 6(3) (2020) 479-488.

[3]. G. A. Putrus, et al., Impact of electric vehicles on power distribution networks, 2009 IEEE Vehicle Power and Propulsion Conference, Dearborn, MI, USA, 2009, pp. 827-831.

[4]. A. Dubey, et al., Electric vehicle charging on residential distribution systems: Impacts and mitigations, IEEE Access 3 (2015) 1871-1893.

[5]. A. Colmenar-Santos, et al., Electric vehicle charging strategy to support renewable energy sources in Europe 2050 low-carbon scenario, Energy 183 (2019) 61-74.

[6]. M. Sathiskumar, et al., A self adaptive hybrid differential evolution algorithm for phase balancing of unbalanced distribution system, Int. J. Electr. Power Energy Syst. 42 (2012) 91-97.

[7]. M. W. Siti, et al., Reconfiguration and load balancing in the LV and MV distribution networks for optimal performance, IEEE Trans. Power Deliv. 22(4) (2007) 2534-2540.

[8]. Y. Fang, et al., Research of active load regulation method for distribution network considering distributed photovoltaic and electric vehicles. J. Eng. 13 (2017) 2444-2448.

[9]. F. Gou, et al., Ordered charging strategy for electric vehicles based on load balancing, 2017 IEEE Conference on Energy Internet and Energy System Integration (EI2), Beijing, China, 2017, pp. 1-5.

[10]. Y. Hu, et al., A Real-time multilevel energy management strategy for electric vehicle charging in a smart electric energy distribution system. Energy Technol. 7 (2019) 1800705.

[11]. B. Wang, et al., Improving hosting capacity of unbalanced distribution networks via robust allocation of battery energy storage systems, IEEE Trans. Power Syst. 36(3) (2021) 2174-2185.

[12]. S. Chen, et al., A game theoretic approach to phase balancing by plug-in electric vehicles in the smart grid, IEEE Trans. Power Syst. 35(3) (2020) 2232-2244.

[13]. S. Sun, et al., Taylor, Phase balancing using energy storage in power grids under uncertainty, IEEE Trans. Power Syst. 31(5) (2016) 3891-3903.

[14]. G. Liu, et al., Distributed energy management for community microgrids considering phase balancing and peak shaving. IET Gener. Transm. Distrib. 13(9) (2019) 1612-1620.

[15]. H. Ramadan, et al., Smart charging and discharging of plug-in electric vehicles for peak shaving and valley filling of the grid power, 2018 Twentieth International Middle East Power Systems Conference (MEPCON), Cairo, Egypt, 2018, pp. 735-739.

[16]. B. Debnath, et al., Optimization of electric vehicle charging to shave peak load for integration in smart grid, 2020 IEEE Region 10 Symposium (TENSYMP), Dhaka, Bangladesh, 2020, pp. 483-488.

[17]. L. Jian, et al., A scenario of vehicle-to-grid implementation and its double-layer optimal charging strategy for minimizing load variance within regional smart grids, Energy Convers. Manag. 78 (2014) 508-517.

[18]. C. S. Lai, et al., A distributed transaction method for mitigating three-phase imbalance by scheduling electric vehicle charging, in 2021 6th Asia Conference on Power and Electrical Engineering (ACPEE), Chongqing, China, 2021, pp. 736-740.

[19]. Z. Huang, et al., A novel power market mechanism based on blockchain for electric vehicle charging stations, Electronics 10 (3), 307, Jan 2021.

[20]. Y. Wu, et al., Optimal battery capacity of grid-connected PV-battery systems considering battery

degradation, Renew. Energ. 181 (2022) 10-23.
[21]. S. Boyd, et al., Distributed optimization and statistical learning via the alternating direction method of multipliers, Foundations and Trends in Machine Learning, 3(1) (2010) 1–122.
[22]. “IEEE distribution test feeders,” Accessed: Nov. 2021. [Online]. Available: https://site.ieee.org/pes-testfeeders/resources/
[23]. S. A. Q. Mohammed and J. W. Jung, A comprehensive state-of-the-art review of wired/wireless charging technologies for battery electric vehicles: Classification/common topologies/future research issues, IEEE Access (2021) 19572-19585.
[24]. C. S. Lai, et al., Economic and financial appraisal of novel large-scale energy storage technologies, Energy 214 (2021) 118954.
[25]. W. H. Kersting, The computation of neutral and dirt currents and power losses, IEEE PES Power Systems Conference and Exposition, 1 (2004) 213-218.